CONDENSED MATTER PHYSICS

Highly efficient coherent amplification of zero-field spin waves in YIG nanowaveguides

Kirill O. Nikolaev[1]†, Stephanie R. Lake[2]†, Bikash Das Mohapatra[2]†, Georg Schmidt[2,3], Sergej O. Demokritov[1], Vladislav E. Demidov[1]*

Transmission and processing of information at the nanoscale using spin waves and their quanta—magnons—offer numerous advantages and opportunities that make it a promising next-generation technology for integrated electronics. The main challenges that still need to be addressed to ensure high competitiveness of magnonic devices include finding ways to efficiently amplify spin waves in nanostructures and developing nanocircuits that can operate without the need for an external bias magnetic field. Here, we demonstrate how these two challenges can be solved using nanowaveguides fabricated from a low-loss magnetic insulator. We show that using local parametric pumping with a power of only a few milliwatts, one can achieve coherent amplification of spin-wave pulses by more than two orders of magnitude at zero bias magnetic field. Our results provide a simple solution to problems that have long prevented the implementation of efficient integrated magnonic circuits.

INTRODUCTION

The emergent field of magnonics considers the use of spin waves propagating in magnetic nanostructures and networks for low-energy transmission of signals and processing of information (*1*). Owing to short wavelengths, down to a few tens of nanometers (*2*–*4*), and excellent controllability by magnetic and electric fields (*5*–*10*), spin waves offer many important opportunities for the implementation of efficient integrated devices and circuits (*11*–*13*). Moreover, because of the rich spectrum of nonlinear phenomena (*14*–*18*), spin waves provide a unique platform for advanced information processing including reservoir and neuromorphic computing and Ising machines (*19*–*22*).

The benefits of spin waves are strongly compromised by two important factors. First, in nanostructured magnonic waveguides, spin waves exhibit relatively short propagation lengths. Even in nanostructures fabricated from ultra–low-loss magnetic insulator—yttrium iron garnet (YIG) (*23*–*25*)—the propagation length typically does not exceed several tens of micrometers (*26*–*28*). Therefore, the implementation of complex magnonic nanocircuits constituted by many cascaded devices necessarily requires a periodic recovery or amplification of spin-wave signals. This amplification is also crucial, for example, for the functioning of spin-wave Ising machines, whose performance is limited by the number of distinguishable time-multiplexed spin-wave pulses (*22*). Although these problems are well recognized, until now there was no efficient solution for amplification of spin waves at the nanoscale. Recently, it was shown that the nanoscale amplification can be achieved using spin-transfer torque phenomena (*27*), stimulated magnon scattering (*26*), or bistability phenomena (*28*). However, the achieved gains did not exceed a factor of 5 to 6. In addition, the last two mechanisms lack coherence, i.e., the important phase information is lost during amplification.

Another mechanism, which can be used for amplification of spin waves, is the parametric pumping (*29*). This mechanism was intensively studied in the past in macroscopic millimeter-scale spin-wave devices and was shown to enable large gains up to a factor of several hundreds (*30*–*33*). However, previous attempts to apply this mechanism to microscopic structures have had limited success. Reasonable parametric gains could only be observed in transition-metal ferromagnetic structures (*34*), where the achieved amplification was completely compromised by large losses typical for these materials. In contrast, in nanostructures fabricated from low-loss magnetic insulators, such as YIG, the parametric mechanism could only be used to generate spin waves (*35*), while no parametric amplification has been demonstrated so far.

In addition to the missing efficient amplification of spin waves, nanomagnonics also strongly suffers from the requirement to apply static bias magnetic fields, which is needed to operate most of the spin-wave devices. This requirement greatly complicates the practical implementation of devices and circuits, as it requires the integration of space- and energy-consuming magnetic systems. Accordingly, considerable efforts have been directed toward finding ways to achieve propagation of spin waves at zero magnetic field. Although a number of approaches to solving this problem have been demonstrated (*36*–*39*), most of them require the use of magnetic materials with large magnetic losses. Only recently, it was shown (*40*) that zero-field transmission of spin waves can be realized in nanosized waveguides fabricated from low-loss YIG films. These waveguides have been proven to exhibit a highly stable uniform magnetic state at zero bias magnetic field and support the propagation of spin waves with long propagation lengths. These features make such waveguides promising building blocks for the development of complex magnonic devices and networks.

In this work, we experimentally demonstrate that spin waves propagating in YIG nanowaveguides at zero bias magnetic field can be efficiently amplified using a parametric pumping localized in an active region as small as 2 μm in length. We show that a pumping power of only 4 mW is sufficient to fully compensate for the losses experienced by spin-wave pulses over the propagation distance of 10 μm. At the highest power of 15 mW used in our experiment, we achieve gains of more than two orders of magnitude, which are mainly limited by the onset of nonlinear phenomena at large intensities of the amplified pulses. The achieved gains are sufficient to completely

[1]Institute of Applied Physics, University of Muenster, 48149 Muenster, Germany. [2]Institut für Physik, Martin-Luther-Universität Halle-Wittenberg, 06120 Halle, Germany. [3]Interdisziplinäres Zentrum für Materialwissenschaften, Martin-Luther-Universität Halle-Wittenberg, 06120 Halle, Germany.
*Corresponding author. Email: demidov@uni-muenster.de
†These authors contributed equally to this work.

compensate the spin-wave losses at propagation distances of more than 60 μm using one single local amplifier. Using phase-resolved measurements, we directly prove that the studied amplification process does not disturb the phase coherence of spin-wave pulses. Therefore, it can also be used in advanced magnonic circuits, taking advantage of the possibility of encoding the information into the phase of spin waves and using interference phenomena for information processing.

RESULTS

Studied system and approach

Figure 1 schematically illustrates the idea of the experiment. Spin-wave pulses with the carrier frequency f_s propagate in a 500-nm-wide and 80-nm-thick waveguide fabricated from a YIG film prepared by the pulsed laser deposition (*25*). The measurements are performed at zero static magnetic field. Under these conditions, the static magnetization in the waveguide is spatially uniform and is aligned parallel to the axis of the waveguide (*40*), which corresponds to the propagation configuration of the so-called backward-volume spin waves (*29*).

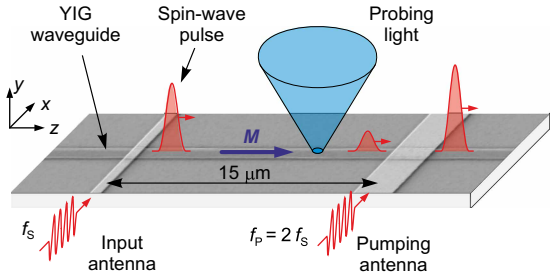

Fig. 1. Schematics of the experiment. Spin-wave pulses with the carrier frequency f_s propagate in a 500-nm-wide and 80-nm-thick YIG waveguide at zero bias magnetic field. The pulses are amplified using a pulsed parametric pumping field with a frequency $f_p = 2\,f_s$, which is generated by a 2-μm-wide pumping antenna. The propagation and amplification of the spin-wave pulses are studied with spatial and temporal resolution using BLS spectroscopy.

Spin waves are inductively excited by applying 20-ns-long pulses of microwave current through a 500-nm-wide and 200-nm-thick input Au antenna. After traveling 15 μm along the waveguide, the pulses encounter another antenna with a width of 2 μm. This antenna is used for parametric amplification. To implement the amplification, we apply microwave pulses to this antenna at a frequency that is twice the frequency of the signal carried by spin waves—the parametric pumping. A dynamic magnetic field at this frequency cannot linearly excite magnetic dynamics. Instead, it serves as a periodic modulation of the system parameters, which is known to lead to compensation of magnetic damping (*30*–*32*). At sufficiently high powers of the pumping signal, the damping becomes negative, which leads to an amplification of the spin-wave pulse passing through the pumping region.

We study the propagation and amplification of the spin-wave pulses using space- and time-resolved microfocus Brillouin light scattering (BLS) spectroscopy (*41*). We focus probing laser light into a diffraction-limited spot on the YIG waveguide (see Fig. 1) and analyze the modulation of this light due to its scattering from spin waves. The detected BLS intensity is proportional to the spin-wave intensity at the position of the probing-light spot, which provides the opportunity to directly observe the propagation of spin-wave pulses with high spatial resolution.

Evidence of parametric amplification

Figure 2 illustrates the main achievement of our work—highly efficient local amplification of spin-wave pulses. Here, we use signal pulses with the frequency $f_s = 1.5$ GHz, which corresponds to the middle of the spin-wave band at zero static magnetic field (see Supplementary Text and fig. S1). First, we analyze the propagation of pulses without applying parametric pumping (Fig. 2, A and B). We move the probing-light spot along the waveguide with a step of 500 nm and record the temporal traces of the BLS intensity at different z positions. The results of these measurements are presented in Fig. 2A as a color map in space-time coordinates. Representative temporal profiles of the spin-wave pulses recorded at points A ($z = 0$), B ($z = 15.5$ μm), and C ($z = 30$ μm) are shown in Fig. 2B. As seen from these data, despite the ultimately low magnetic damping in YIG, the spin-wave

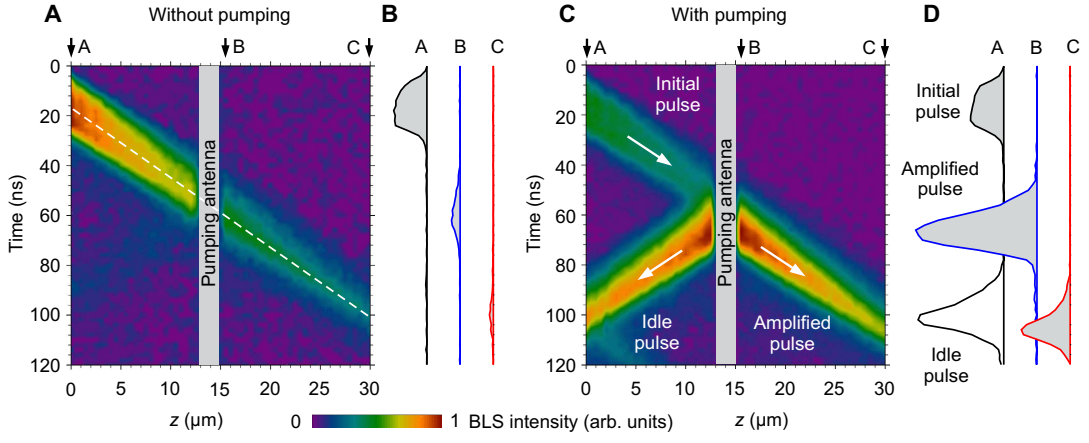

Fig. 2. Propagation and amplification of spin-wave pulses. (**A** and **C**) Color maps of spin-wave intensity in space-time coordinates. (A) shows the data obtained without pumping. (C) shows the data obtained with pumping at a power of $P_p = 10$ mW. arb., arbitrary. (**B** and **D**) show representative temporal profiles of spin-wave pulses recorded at points A ($z = 0$), B ($z = 15.5$ μm), and C ($z = 30$ μm) without (B) and with (D) pumping. The dashed line in (A) marks the propagation of the center of the spin-wave pulse. The slope of the line corresponds to the group velocity of $v_g = 0.36$ μm/ns. The data are obtained at zero bias magnetic field. The frequency of the spin-wave pulses is $f_s = 1.5$ GHz. The power of the signal applied to the input antenna is $P_s = 0.1$ mW.

pulse experiences a noticeable decay as it propagates in the waveguide: after a travel distance of 30 μm, its intensity decreases by about a factor of 10. From the slope of the dashed line in Fig. 2A, we determine the group velocity of the spin waves—$v_g = 0.36$ μm/ns. At such velocity, the center of the pulse passes through the 2-μm-wide pumping region in 6 ns. Accordingly, we choose the duration of the pumping pulse to be 26 ns, so that the pumping starts when the leading edge of the 20-ns-wide signal pulse reaches the pumping region and ends when its trailing edge leaves this region.

Figure 2 (C and D) shows the results obtained when applying a signal with a frequency $f_p = 2 f_s = 3.0$ GHz and a power of $P_p =$ 10 mW to the pumping antenna. Simple comparison of these data with the data in Fig. 2 (A and B) indicates the high efficiency of the parametric amplification. In particular, the intensity of the pulse at point B (directly behind the pumping antenna) increases by a factor of about 16. Moreover, the intensity of the pulse at point C ($z = 30$ μm) is now larger than the intensity of the initially excited pulse at point A ($z = 0$). In other words, in this representative example, the complete compensation of spin-wave losses corresponding to the propagation distance of 30 μm is achieved.

The data of Fig. 2C also show the excitation by the parametric pumping of the so-called idle pulse, which is typical for all parametric amplifiers. The parametric amplification can be viewed as the stimulated splitting of the photon of the pumping field into two magnons with half the frequency (*29*). To satisfy the conservation of momentum, these two magnons must have opposite wave vectors, i.e., propagate in opposite directions. This leads to a formation of the idle pulse propagating oppositely to the amplified signal pulse. In principle, the generation of the idle pulses may lead to some limitations if the idle pulses interact with subsequent signal pulses. However, this interaction is only possible in a strongly nonlinear regime and requires large amplitudes of the pulses at the interaction point, which can be easily avoided. In addition, we note that the generation of idle pulses can also be used for certain applications (*42*).

To better quantify the demonstrated amplification, we show in Fig. 3 the spatial dependences of the peak intensity of the initial and the amplified pulses. As seen from these data, the intensity always shows a clear exponential decay (note the logarithmic scale of the vertical axis) characterized by the propagation length of 28 μm, which is typical for zero-field backward-volume waves in the waveguides used (*40*). Extrapolating the exponential fit of the data for the initial pulse beyond the pumping region (dashed line in Fig. 3), one can see that the presence of the pumping antenna results in a small drop in intensity. This drop is due to the unavoidable reflection and absorption of spin-wave energy by the pumping antenna. We emphasize that this drop is insignificant compared to the increase in intensity achieved using the parametric pumping.

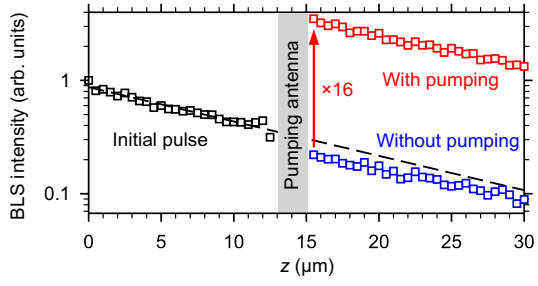

Fig. 3. Quantitative characterization of the amplification. Spatial dependences of the peak intensity of spin-wave pulses with and without pumping. The dashed line shows the exponential fit of the data in the range $z = 0$ to 12 μm. The slope of the line corresponds to the propagation length of the spin waves of 28 μm. The arrow illustrates the increase in intensity by a factor of 16 due to parametric amplification. The data are obtained at zero bias magnetic field. The frequency of the spin-wave pulses is $f_s = 1.5$ GHz. The power of the signal applied to the input antenna is $P_s = 0.1$ mW. The pumping power is $P_p = 10$ mW.

Power dependences of the parametric gain

We now discuss how the observed amplification depends on the pumping and signal power. Figure 4A shows the dependences of the BLS signal detected at the output of the amplifier (point B in Fig. 2A) as a function of the pumping power P_p for two different powers of the signal pulse $P_s = 0.05$ and 0.1 mW. The data in Fig. 4A show that the intensity of the amplified pulse increases approximately exponentially (note the logarithmic scale of the vertical axis) with increasing pumping power $P_p < 10$ mW and then tends to saturate. At the maximum pumping power used in the experiment ($P_p = 15$ mW), the intensity of the amplified pulses becomes almost independent of the power of the signal pulse. This indicates that the maximum intensity of the amplified pulse is limited by the onset of nonlinear phenomena, such as the nonlinear damping and nonlinear shift of the spin-wave spectrum, leading to the reduction of the efficiency of the interaction of spin waves with the pumping field (*29*). This nonlinear limitation results in a dependence of the parametric gain on the intensity of the initial pulse at large P_p. In particular, at $P_p = 15$ mW, the gain is limited to about 28, if the input power of $P_s = 0.1$ mW is used. However, when the input power is reduced to $P_s = 0.05$ mW, an almost twice the gain (≈55) can be achieved.

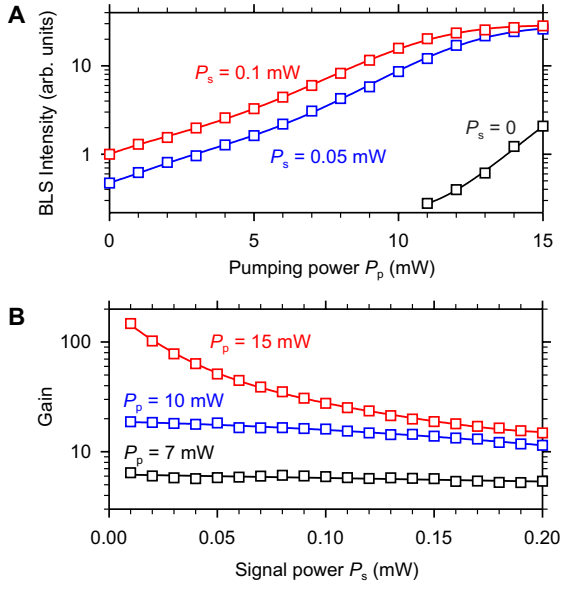

Fig. 4. Power dependences of the parametric amplification. (**A**) Dependences of the BLS signal detected at the output of the amplifier (point B in Fig. 2B) on the pumping power P_p for different powers of the signal pulse P_s, as labeled. (**B**) Dependences of the parametric gain on the signal power P_s for different pumping powers P_p, as labeled. Symbols show the experimental data. Curves are guides for the eye. The data are obtained at zero bias magnetic field. The frequency of the spin-wave pulses is $f_s = 1.5$ GHz.

Every amplifier amplifies not only the signal applied to its input but also the noise that is present in any system at finite temperatures. This also applies to the studied parametric amplification mechanism. In addition to amplifying coherent signal pulses, the parametric process causes amplification of incoherent thermal magnetic fluctuations. To characterize this parasitic effect, we measure the BLS intensity at the output of the amplifier without applying any signal to the input antenna (see data for $P_s = 0$ in Fig. 4A). As seen from these data, incoherent parametric generation can be detected only at $P_p >$ 10 mW, and the intensity of the corresponding signal is small even at the largest used pumping power. This is not surprising because the initial intensities of thermal fluctuations are negligible compared to the intensities of the coherent pulses excited by the input antenna. Therefore, their amplification to a considerable level during a 26-ns-long pumping pulse requires high gains, which are only achieved at high P_p. In the case $P_p = 10$ mW, illustrated in Figs. 2 and 3, the amplified incoherent fluctuations have intensities below the detection threshold and can be neglected.

Figure 4B characterizes the dependence of the parametric gain on the input power in more detail. At small $P_p = 7$ mW, far below saturation, the gain is almost independent of the signal power. At $P_p = 10$ mW, the gain already decreases noticeably, as the signal power increases from 0.01 to 0.2 mW. Last, at $P_p = 15$ mW, the gain becomes very sensitive to the signal power. At the smallest $P_s =$ 0.01 mW, the gain reaches a value of more than 100. These observations allow us to formulate guidelines for the optimum use of parametric amplification in magnonic circuits. In particular, they show that the efficiency of parametric amplification is particularly high in the small-signal regime. In practice, this situation is realized, for example, if local amplification is used to restore strongly attenuated spin-wave pulses that have traveled a long distance. Given the measured propagation length of 28 μm, the intensity of the initially excited spin-wave pulse decreases by a factor of 100 after traveling 64 μm. It can be expected that under these conditions, the signal intensity is small enough to achieve gains greater than 100 using $P_p = 15$ mW. In other words, by placing parametric amplifiers every 64 μm and using the pumping with the power of 15 mW, one can completely compensate the propagation losses of spin waves in a spatially extended magnonic circuit. Depending on the requirements of a particular application, one can also place amplifiers with smaller spacing and use lower pumping powers. For example, if the amplifiers are placed every 10 μm, then the propagation losses can be completely compensated using the power as small as $P_p = 4$ mW.

Effects of the frequency detuning

The need for a microwave pumping with a frequency exactly twice the frequency of the amplified signal can be viewed as a limiting factor for the practical use of the parametric amplification mechanism. We emphasize, however, that this strict requirement only applies if the frequency and wave vector of the pumping-field photon are strictly defined. In the practically relevant case considered in our study, the pumping is applied in the form of pulses, which leads to frequency uncertainty. In addition, the pumping field is spatially localized, which results in an uncertainty of its wave vector. Under these conditions, amplification remains efficient even if the pumping frequency deviates from 2 f_s. This is illustrated in Fig. 5, which shows the dependence of the parametric gain on the detuning of the pumping frequency from 2 f_s. As seen from these data, the gain remains within half of its maximum value over a frequency band, which is as large as 0.1 GHz. This band can be further extended using shorter pulses and/or stronger spatial localization of the pumping field.

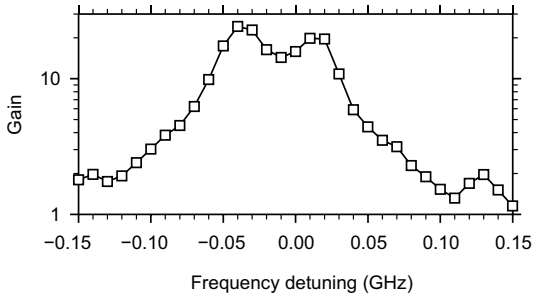

Fig. 5. Effects of the frequency detuning. Dependence of the gain on the detuning of the pumping frequency from 2 f_s. The data are obtained at zero bias magnetic field. The frequency of the signal is f_s = 1.5 GHz. The power of the signal applied to the input antenna is $P_s = 0.1$ mW. The pumping power is $P_p = 10$ mW.

Coherence of the amplification process

One of the important advantages of wave-based transmission and processing of information is that the information can be encoded not only into intensity but also into the phase of the waves. Therefore, a key requirement for the amplification or recovery process is that it does not lead to a loss of phase information. To show that this is the case for the parametric process under study, we perform BLS measurements with phase resolution (*41*). To achieve sensitivity of the BLS apparatus to the phase of spin waves, we exploit the interference of the light scattered from the spin waves with reference light modulated by the microwave signal used to excite the input spin-wave pulses. The resulting signal is then proportional to $A_{sw}(z)\cos[\Delta\varphi(z)]$, where A_{sw} is the amplitude of the spin wave at the observation point z and $\Delta\varphi$ is the shift of its phase relative to the phase of the microwave signal at the input antenna.

Figure 6A shows the phase-resolved spatial profiles of the spin-wave pulses recorded at times $t = 30$ and 85 ns. At $t = 30$ ns, the spin-wave pulse is located between the input antenna and the pumping antenna, i.e., it has not yet undergone amplification. At $t = 85$ ns, the entire amplified pulse has already left the pumping region. As seen from the data in Fig. 5A, both the initial and amplified pulses exhibit clear periodic oscillations, which are determined by the oscillations of the term $\cos[\Delta\varphi(z)]$. This fact already indicates that the phase of the amplified pulse is locked to that of the initial pulse. Because in BLS measurements the signal is averaged over a very large number of pulses, the term $\cos[\Delta\varphi(z)]$ would average to zero if there were no phase coherence. This averaging is seen for the idle pulse: although the intensities of the amplified and the idle pulse are almost the same (see Fig. 2D), we do not observe an oscillating signal in Fig. 6A on the left from the pumping antenna, indicating that the phase of the idle pulse is not locked to that of the initial pulse. Instead, we observe a weak nonoscillating signal. The latter is caused by a small contribution to the measured signal proportional to the spin-wave intensity, which is difficult to completely exclude. We emphasize that this result is consistent with the concept of the parametric amplification process as a stimulated splitting of a pumping-field photon into two magnons. It is known that such a process conserves the sum of the phases of the three involved quasiparticles (*29*). Because the splitting is stimulated by the signal pulse, the phase of the generated magnon contributing to the amplified pulse is automatically synchronized with the phase of

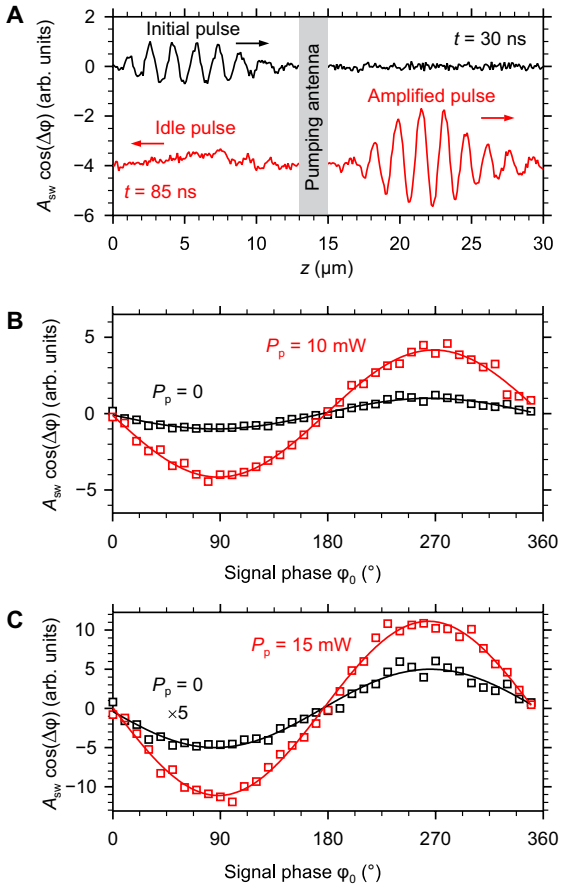

Fig. 6. Evidence for the coherence of the amplification process. (**A**) Phase-resolved spatial profiles of the spin-wave pulse recorded before ($t = 30$ ns) and after ($t = 85$ ns) amplification. Curves are vertically shifted for clarity. The data are recorded at $P_s = 0.1$ mW and $P_p = 10$ mW. (**B** and **C**) Dependences of the phase-resolved signal on the phase of the microwave signal applied to the input antenna, recorded at the output of the amplifier with and without pumping. The data in (B) are recorded at $P_s = 0.1$ mW and $P_p = 10$ mW. The data in (C) are recorded at the lowest used signal power $P_s = 0.01$ mW and the highest used pumping power $P_p = 15$ mW. Symbols show the experimental data. Curves are the fits of the data by a sinusoidal function. The data are obtained at zero bias magnetic field. The frequency of the spin-wave pulses is $f_s = 1.5$ GHz.

the signal. However, because the pumping field is not phase locked to the input signal, the phase of the idle magnon is undefined. In our experiments, we intentionally do not synchronize the phase of the pumping with that of the amplified pulses to demonstrate that amplification does not require such synchronization. The absence of this requirement is an important advantage of the parametric process because it greatly simplifies its practical implementation. As shown above, the lack of synchronization does not affect the phase coherence of the amplified pulse. It only results in an undefined phase of the idle pulse, which is not important for the amplification process.

The phase-resolved profiles in Fig. 6A also allow us to directly determine the wave number k_0 of the carrier wave for the initial and amplified pulses. We use the Fourier transformation of the data and obtain for both pulses $k_0 = 3.98\ \mu m^{-1}$, which corresponds to the wavelength of 1.58 μm. This result indicates that the amplification process not only preserves the phase of the signal but also does not affect the wavelength of the carrier spin wave.

We now use phase-resolved measurements to demonstrate that the observed intensity gain (Fig. 4B) is dominated by the amplification of the coherent component of the signal pulse. To prove this, we sweep the phase of the microwave signal applied to the input antenna φ_0 from 0° to 360°, keeping the phase of the reference modulation constant, and carry out interference measurements at point B ($z = 15.5$ μm) at the output of the parametric amplifier. Figure 6B shows the resulting interference curves recorded with and without pumping ($P_s = 0.1$ mW and $P_p = 10$ mW). As expected, both of them exhibit sinusoidal oscillation. The amplitude of this oscillation is proportional to the amplitude of the coherent component, phase locked to the input microwave signal. We fit the data with a sinusoidal function and find that the ratio between the oscillation amplitudes is 4. This corresponds to the intensity gain of 16, which is equal to the gain value obtained in the intensity measurements, indicating that the amplification is fully coherent.

Next, we prove that the coherence is preserved even at the lowest used signal power $P_s = 0.01$ mW and the largest used pumping power $P_p = 15$ mW (Fig. 6C), which corresponds to the case of the ultimate gain of 147 observed in the intensity measurements (Fig. 4B). Under these extreme conditions, the intensity of parametrically amplified incoherent fluctuations detected at the output of the amplifier without applying any signal to the input antenna accounts for 18% of the intensity detected in the presence of the input signal. Accordingly, the coherent gain is expected to be ~82% of the total observed intensity gain. Fitting of the phase-resolved data (Fig. 6C) yields a ratio between the oscillation amplitudes of 11. This corresponds to the intensity gain of 121, which agrees well with the estimates given above. These results indicate that the obtained gains characterize the amplification of the coherent component and that the amplification process remains highly coherent even for the weakest signals used in our experiments.

Effects of the bias magnetic field

Last, we demonstrate that operating the parametric amplifier at zero bias magnetic field is essential to achieve highly efficient amplification. To do this, we apply a static magnetic field parallel to the axis of the waveguide and determine the maximum achievable parametric gain from measurements similar to those shown in Fig. 4. To ensure that the experimental conditions are approximately the same at different fields, we choose the signal frequency in such a way that the wavelength of the signal spin wave remains approximately constant. Figure 7 shows the obtained field dependence of the maximum gain. As seen from these data, the gain decreases by more than an order of magnitude already when a field of 250 Oe is applied and continues to quickly decrease at higher fields. We associate these observations with the influence of two factors. First, an increase in the bias magnetic field results in a shift of the spin-wave band toward higher frequencies, which leads to an increase in the spin-wave relaxation rate. Second, as shown by micromagnetic simulations (see Supplementary Text and fig. S2), an increase in the bias field results in a noticeable decrease in the ellipticity of the magnetization precession. Both of these factors increase the power threshold of the parametric process (*29*) and lead to a strong decrease in the gain at a given power of the parametric pumping. These results indicate that the use of zero-field spin waves not only eliminates the need for space- and energy-consuming magnetic systems but also allows one to maximize the efficiency of the parametric amplification mechanism, making it suitable for practical applications.

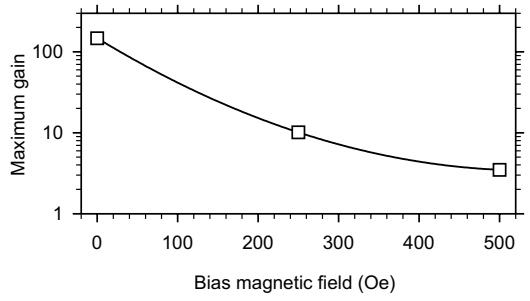

Fig. 7. Effects of the bias magnetic field. Dependence of the maximum achieved gain on the bias magnetic field. The pumping power is $P_p = 15$ mW. Symbols show experimental data. The curve is a guide for the eye.

DISCUSSION

In summary, we experimentally demonstrated a highly efficient approach to address the key challenges in nanomagnonics. We show that spin waves propagating at zero bias magnetic field in waveguides made from low-loss magnetic insulators can be efficiently amplified by local parametric pumping and that this amplification process preserves the phase information carried by spin waves. Our results pave the way for the realization of complex magnonic circuits for nanoscale transmission and processing of information, which can operate without a bias magnetic field and do not require energy-inefficient conversion of spin waves into electric currents to recover spin-wave signals.

MATERIALS AND METHODS

Sample fabrication

The YIG waveguides are fabricated using electron beam lithography, pulsed laser deposition, and lift-off. Electron beam lithography is performed using a two-layer poly(methyl methacrylate) (PMMA) resist spin coated on a <111>-oriented GGG substrate. The PMMA is covered by an ultrathin gold film to provide a conducting surface and to avoid charging during the exposure. After electron beam exposure (30 kV), the gold is removed using a potassium iodide solution. The PMMA is developed in pure isopropanol. Possible residual resist in the developed areas is removed using oxygen plasma. A nominally 100-nm-thick YIG film is deposited at room temperature by pulsed laser deposition using a process developed by Hauser *et al.* (*25*). After lift-off in acetone, the sample is annealed in oxygen for 3 hours at 800°C. Wet etching in phosphoric acid removes ~20 nm of YIG and provides smooth edges. For high-frequency measurements, microstrip antennas are deposited on top of the YIG waveguides using a similar process but replacing the pulsed laser deposition of YIG with e-gun evaporation of 10 nm of titanium and 200 nm of gold and discarding the annealing step after lift-off.

Microfocus BLS measurements

All measurements are performed in a pulsed regime. The width of the pulses used for the excitation of spin waves is 20 ns, and their repetition period is 500 ns. To detect propagating spin-wave pulses with spatial and temporal resolution, we use inelastic scattering of laser light from spin waves. Light with a wavelength of 473 nm and a power of 0.25 mW is generated by a single-frequency laser with a linewidth < 5 MHz. We use a high-performance microscope objective lens with a magnification of 100 and a numerical aperture of 0.9 to focus the laser light into a diffraction-limited spot, which ensures high spatial resolution of the measurements. The position of the probing spot is monitored and actively stabilized using a home-built digital microscope. The scattered light is analyzed using a six-pass Fabry-Perot interferometer and a high-sensitivity single-photon detector. By determining the delay of the detected photons of the scattered light relative to microwave pulses used to excite spin waves, we achieve a temporal resolution of about 1 ns. To obtain sensitivity of the technique to the phase of spin waves, we use the interference of scattered light with the reference light. The reference light is modulated at the frequency of spin waves using a broadband electro-optical modulator.

Supplementary Materials

This PDF file includes:

Supplementary Text
Figs. S1 and S2
References

REFERENCES AND NOTES

1. B. Flebus, D. Grundler, B. Rana, Y. Otani, I. Barsukov, A. Barman, G. Gubbiotti, P. Landeros, J. Akerman, U. Ebels, P. Pirro, V. E. Demidov, K. Schultheiss, G. Csaba, Q. Wang, F. Ciubotaru, D. E. Nikonov, P. Che, R. Hertel, T. Ono, D. Afanasiev, J. Mentink, T. Rasing, B. Hillebrands, S. V. Kusminskiy, W. Zhang, C. R. Du, A. Finco, T. van der Sar, Y. K. Luo, Y. Shiota, J. Sklenar, T. Yu, J. Rao, The 2024 magnonics roadmap. *J. Phys. Condens. Matter* **36**, 363501 (2024).
2. H. Yu, O. d'Allivy Kelly, V. Cros, R. Bernard, P. Bortolotti, A. Anane, F. Brandl, F. Heimbach, D. Grundler, Approaching soft x-ray wavelengths in nanomagnet-based microwave technology. *Nat. Commun.* **7**, 11255 (2016).
3. C. Liu, J. Chen, T. Liu, F. Heimbach, H. Yu, Y. Xiao, J. Hu, M. Liu, H. Chang, T. Stueckler, S. Tu, Y. Zhang, Y. Zhang, P. Gao, Z. Liao, D. Yu, K. Xia, N. Lei, W. Zhao, M. Wu, Long-distance propagation of short-wavelength spin waves. *Nat. Commun.* **9**, 738 (2018).
4. V. Sluka, T. Schneider, R. A. Gallardo, A. Kákay, M. Weigand, T. Warnatz, R. Mattheis, A. Roldán-Molina, P. Landeros, V. Tiberkevich, A. Slavin, G. Schütz, A. Erbe, A. Deac, J. Lindner, J. Raabe, J. Fassbender, S. Wintz, Emission and propagation of 1D and 2D spin waves with nanoscale wavelengths in anisotropic spin textures. *Nat. Nanotechnol.* **14**, 328–333 (2019).
5. K. Vogt, F. Y. Fradin, J. E. Pearson, T. Sebastian, S. D. Bader, B. Hillebrands, A. P. Hoffmann, H. Schultheiss, Realization of a spin-wave multiplexer. *Nat. Commun.* **5**, 3727 (2014).
6. M. Evelt, L. Soumah, A. B. Rinkevich, S. O. Demokritov, A. Anane, V. Cros, J. Ben Youssef, G. de Loubens, O. Klein, P. Bortolotti, V. E. Demidov, Emission of coherent propagating magnons by insulator-based spin-orbit-torque oscillators. *Phys. Rev. Appl.* **10**, 041002 (2018).
7. H. Qin, R. B. Holländer, L. Flajšman, F. Hermann, R. Dreyer, G. Woltersdorf, S. van Dijken, Nanoscale magnonic Fabry-Perot resonator for low-loss spin-wave manipulation. *Nat. Commun.* **12**, 2293 (2021).
8. T. Nozaki, Y. Shiota, S. Miwa, S. Murakami, F. Bonell, S. Ishibashi, H. Kubota, K. Yakushiji, T. Saruya, A. Fukushima, S. Yuasa, T. Shinjo, Y. Suzuki, Electric-field-induced ferromagnetic resonance excitation in an ultrathin ferromagnetic metal layer. *Nat. Phys.* **8**, 491–496 (2012).
9. R. Verba, M. Carpentieri, G. Finocchio, V. Tiberkevich, A. Slavin, Excitation of spin waves in an in-plane-magnetized ferromagnetic nanowire using voltage-controlled magnetic anisotropy. *Phys. Rev. Appl.* **7**, 064023 (2017).
10. S. Choudhury, A. K. Chaurasiya, A. K. Mondal, B. Rana, K. Miura, H. Takahashi, Y. Otani, A. Barman, Voltage controlled on-demand magnonic nanochannels. *Sci. Adv.* **6**, eaba5457 (2020).
11. G. Csaba, A. Papp, W. Porod, Perspectives of using spin waves for computing and signal processing. *Phys. Lett. A* **381**, 1471–1476 (2017).
12. A. Mahmoud, F. Ciubotaru, F. Vanderveken, A. V. Chumak, S. Hamdioui, C. Adelmann, S. Cotofana, Introduction to spin wave computing. *J. Appl. Phys.* **128**, 161101 (2020).
13. Q. Wang, G. Csaba, R. Verba, A. V. Chumak, P. Pirro, Nanoscale magnonic networks. *Phys. Rev. Appl.* **21**, 040503 (2024).
14. A. V. Sadovnikov, S. A. Odintsov, E. N. Beginin, S. E. Sheshukova, Y. P. Sharaevskii, S. A. Nikitov, Toward nonlinear magnonics: Intensity-dependent spin-wave switching in insulating side-coupled magnetic stripes. *Phys. Rev. B* **96**, 144428 (2017).
15. H. Merbouche, B. Divinskiy, K. O. Nikolaev, C. Kaspar, W. H. P. Pernice, D. Gouéré, R. Lebrun, V. Cros, J. Ben Youssef, P. Bortolotti, A. Anane, S. O. Demokritov, V. E. Demidov, Giant nonlinear self-phase modulation of large-amplitude spin waves in microscopic YIG waveguides. *Sci. Rep.* **12**, 7246 (2022).

16. R. Dreyer, A. F. Schäffer, H. G. Bauer, N. Liebing, J. Berakdar, G. Woltersdorf, Imaging and phase-locking of non-linear spin waves. *Nat. Commun.* **13**, 4939 (2022).
17. Q. Wang, R. Verba, B. Heinz, M. Schneider, O. Wojewoda, K. Davídková, K. Levchenko, C. Dubs, N. J. Mauser, M. Urbánek, P. Pirro, A. V. Chumak, Deeply nonlinear excitation of self-normalized short spin waves. *Sci. Adv.* **9**, eadg4609 (2023).
18. K. O. Nikolaev, S. R. Lake, G. Schmidt, S. O. Demokritov, V. E. Demidov, Resonant generation of propagating second-harmonic spin waves in nano-waveguides. *Nat. Commun.* **15**, 1827 (2024).
19. S. Watt, M. Kostylev, Reservoir computing using a spin-wave delay-line active-ring resonator based on yttrium-iron-garnet film. *Phys. Rev. Appl.* **13**, 034057 (2020).
20. A. Papp, W. Porod, G. Csaba, Nanoscale neural network using non-linear spin-wave interference. *Nat. Commun.* **12**, 6244 (2021).
21. L. Körber, C. Heins, T. Hula, J.-V. Kim, S. Thlang, H. Schultheiss, J. Fassbender, K. Schultheiss, Pattern recognition in reciprocal space with a magnon-scattering reservoir. *Nat. Commun.* **14**, 3954 (2023).
22. A. Litvinenko, R. Khymyn, V. H. González, R. Ovcharov, A. A. Awad, V. Tyberkevych, A. Slavin, J. Åkerman, A spinwave Ising machine. *Commun. Phys.* **6**, 227 (2023).
23. H. Chang, P. Li, W. Zhang, T. Liu, A. Hoffmann, L. Deng, M. Wu, Nanometer-thick yttrium iron garnet films with extremely low damping. *IEEE Magn. Lett.* **5**, 6700104 (2014).
24. H. Yu, O. d'Allivy Kelly, V. Cros, R. Bernard, P. Bortolotti, A. Anane, F. Brandl, R. Huber, I. Stasinopoulos, D. Grundler, Magnetic thin-film insulator with ultra-low spin wave damping for coherent nanomagnonics. *Sci. Rep.* **4**, 6848 (2014).
25. C. Hauser, T. Richter, N. Homonnay, C. Eisenschmidt, M. Qaid, H. Deniz, D. Hesse, M. Sawicki, S. G. Ebbinghaus, G. Schmidt, Yttrium iron garnet thin films with very low damping obtained by recrystallization of amorphous material. *Sci. Rep.* **6**, 20827 (2016).
26. D. Breitbach, M. Schneider, B. Heinz, F. Kohl, J. Maskill, L. Scheuer, R. O. Serha, T. Brächer, B. Lägel, C. Dubs, V. S. Tiberkevich, A. N. Slavin, A. A. Serga, B. Hillebrands, A. V. Chumak, P. Pirro, Stimulated amplification of propagating spin waves. *Phys. Rev. Lett.* **131**, 156701 (2023).
27. H. Merbouche, B. Divinski, D. Gouéré, R. Lebrun, A. El Kanj, V. Cros, P. Bortolotti, A. Anane, S. O. Demokritov, V. E. Demidov, True amplification of spin waves in magnonic nano-waveguides. *Nat. Commun.* **15**, 1560 (2024).
28. Q. Wang, R. Verba, K. Davídková, B. Heinz, S. Tian, Y. Rao, M. Guo, X. Guo, C. Dubs, P. Pirro, A. V. Chumak, All-magnonic repeater based on bistability. *Nat. Commun.* **15**, 7577 (2024).
29. A. G. Gurevich, G. A. Melkov, *Magnetization Oscillations and Waves* (CRC, New York, 1996).
30. A. V. Bagada, G. A. Melkov, A. A. Serga, A. N. Slavin, Parametric interaction of dipolar spin wave solitons with localized electromagnetic pumping. *Phys. Rev. Lett.* **79**, 2137–2140 (1997).
31. P. A. Kolodin, P. Kabos, C. E. Patton, B. A. Kalinikos, N. G. Kovshikov, M. P. Kostylev, Amplification of microwave magnetic envelope solitons in thin yttrium iron garnet films by parallel pumping. *Phys. Rev. Lett.* **80**, 1976–1979 (1998).
32. G. A. Melkov, A. A. Serga, A. N. Slavin, V. S. Tiberkevich, A. N. Oleinik, A. V. Bagada, Parametric interaction of magnetostatic waves with a nonstationary local pump. *J. Exp. Theor. Phys.* **89**, 1189–1199 (1999).
33. P. Chowdhury, P. Dhagat, A. Jander, Parametric amplification of spin waves using acoustic waves. *IEEE Trans. Mag.* **51**, 1300904 (2015).
34. T. Brächer, P. Pirro, T. Meyer, F. Heussner, B. Lägel, A. A. Serga, B. Hillebrands, Parallel parametric amplification of coherently excited propagating spin waves in a microscopic $Ni_{81}Fe_{19}$ waveguide. *Appl. Phys. Lett.* **104**, 202408 (2014).
35. B. Heinz, M. Mohseni, A. Lentfert, R. Verba, M. Schneider, B. Läge, K. Levchenko, T. Brächer, C. Dubs, A. V. Chumak, P. Pirro, Parametric generation of spin waves in nanoscaled magnonic conduits. *Phys. Rev. B* **105**, 144424 (2022).
36. K. Wagner, A. Kákay, K. Schultheiss, A. Henschke, T. Sebastian, H. Schultheiss, Magnetic domain walls as reconfigurable spin-wave nanochannels. *Nat. Nanotechnol.* **11**, 432–436 (2016).
37. A. Haldar, D. Kumar, A. O. Adeyeye, A reconfigurable waveguide for energy-efficient transmission and local manipulation of information in a nanomagnetic device. *Nat. Nanotechnol.* **11**, 437–443 (2016).
38. L. Flajšman, K. Wagner, M. Vaňatka, J. Gloss, V. Křižáková, M. Schmid, H. Schultheiss, M. Urbánek, Zero-field propagation of spin waves in waveguides prepared by focused ion beam direct writing. *Phys. Rev. B* **101**, 014436 (2020).
39. J. Klíma, O. Wojewoda, V. Roučka, T. Molnár, J. Holobrádek, M. Urbánek, Zero-field spin wave turns. *Appl. Phys. Lett.* **124**, 112404 (2024).
40. K. O. Nikolaev, S. R. Lake, G. Schmidt, S. O. Demokritov, V. E. Demidov, Zero-field spin waves in YIG nanowaveguides. *Nano Lett.* **23**, 8719–8724 (2023).
41. V. E. Demidov, S. O. Demokritov, Magnonic waveguides studied by microfocus Brillouin light scattering. *IEEE Trans. Mag.* **51**, 0800215 (2015).
42. G. A. Melkov, A. A. Serga, V. S. Tiberkevich, A. N. Oliynyk, A. N. Slavin, Wave front reversal of a dipolar spin wave pulse in a nonstationary three-wave parametric interaction. *Phys. Rev. Lett.* **84**, 3438–3441 (2000).
43. A. Vansteenkiste, J. Leliaert, M. Dvornik, M. Helsen, F. Garcia-Sanchez, B. Van Waeyenberge, The design and verification of MuMax3. *AIP Adv.* **4**, 107133 (2014).

Acknowledgments
Funding: This work was supported by the Deutsche Forschungsgemeinschaft (DFG; German Research Foundation)—project number 529812702 (K.O.N., G.S., and V.E.D.). The work of S.O.D. was supported by the Deutsche Forschungsgemeinschaft (DFG; German Research Foundation)—SFB 1459/2 2025 – 433682494. **Author contributions:** K.O.N. performed measurements and data analysis. S.R.L. and B.D.M. grew and characterized the films and performed nanofabrication and data analysis. G.S., S.O.D., and V.E.D. formulated the experimental approach and supervised the project. All authors cowrote the manuscript. **Competing interests:** The authors declare that they have no competing interests. **Data and materials availability:** All data needed to evaluate the conclusions in the paper are present in the paper and/or the Supplementary Materials.

Submitted 4 March 2025
Accepted 18 August 2025
Published 17 September 2025
10.1126/sciadv.adx2018